Full Paper

Wiley Online Library

ELECTROANALYSIS

DOI: 10.1002/elan.202060389

Simultaneous Detection of Paracetamol, Ascorbic Acid, and Caffeine Using a Bismuth–Silver Nanosensor

Charlton van der Horst,[a] Bongiwe Silwana,[a] Eric Gil,[b] Emmanuel Iwuoha,[c] and Vernon Somerset*[a]

Celebrating the 65th Birthday of Prof Emmanuel I. Iwuoha: Electrochemistry in Africa

Abstract: The bimetallic nanoparticles of bismuth-silver were used to modify a disk GCE for the simultaneous electrochemical analysis of caffeine (CAF), ascorbic acid (AA), and paracetamol (PAR). The constructed Bi-AgNPs/GCE illustrated strong electrocatalytic activity towards the oxidation of CAF, PAR, and AA. Under the optimum conditions, the sensor provided linearity for PAR, AA, CAF between 2 to 20 μM, 10 to 70 μM, and 2 to 40 μM ($n=3$), respectively. The detection limits for CAF, PAR, and AA was 2.36 μM, 0.155 μM, and 0.697 μM, respectively. The GCE/Bi-AgNPs sensor presented good sensitivity and selectivity for the simultaneous electrochemical analysis of CAF, PAR, and AA.

Keywords: Paracetamol · Ascorbic Acid · Caffeine · Bismuth-Silver Bimetallic Nanoparticles · Differential Pulse Voltammetry

1 Introduction

Over the past years, nanomaterials have been drawing increasing attention due to their excellent properties and structures which makes them attractive for numerous applications in several research fields [1–7]. Owing to its extraordinary properties such as mechanical strength, high electrical conductivity, and large surface area bimetallic nanoparticles has shown great promises in electronic and energy storage applications and the construction of electrochemical sensors and biosensors [8–10]. Bimetallic nanocomposites are used to construct electrochemical and biosensors for applications in the detection of dopamine (DA), ascorbic acid (AA), paracetamol (PAR), nitrite ions, H_2O_2, etc. [11,12].

In the search for new electroactive materials for the development and construction of electrochemical sensors, bismuth has been employed to replace mercury and has achieved great attention for pharmaceutical and metallurgical additives [13,14]. Bismuth can form alloys with many metals and is applied as an agent in high-temperature heat-transfers [15–17]. A study done by Sadok et al. [18] has applied bismuth particles modified with Nafion and drop coated on to a boron-doped diamond electrode. This boron-doped diamond sensor has been employed in the individual and simultaneous voltammetric analysis of PAR and CAF. Fernandes et al. [19] developed a novel electrochemical nanosensor consisting of $MnFe_2O_4$@CNT–N for the electrochemical analysis of PAR, CAF, and ascorbic acid (AA). The $MnFe_2O_4$@CNT–N nanosensor illustrated very good results towards the analysis of selected biomolecules. In the case of silver nanoparticles, it has high dispersion, small particle size (less than 20 nm), high surface area, and are used as antifungal agents and antimicrobial [20].

An effective and important antipyretic analgesic drug such as acetaminophen or PAR or N-acetyl-p-aminophenol is applied worldwide. Doctors prescribed PAR for the treatment of mild to moderate pain related to arthritis, headache, etc. [21] with no harmful side effects. An overdose of PAR will cause nephrotoxic and liver metabolites which lead to renal failure [22]. Belonging to N-methyl derivatives of xanthine, CAF or 1,3,7-trimethylxanthine is a natural alkaloid that occurs in tea leaves, cocoa beans, cola nuts, coffee beans, and other plants. CAF is a flavouring agent and is used in a variety of beverages such as soft drinks and energy drinks. It is also known as a stimulant for the central nervous system. CAF can increase alertness, and reduce fine motor coordination in moderate doses and with high doses cause insomnia, nervousness, headaches, and dizziness [23–25]. In the case of AA, this is an important substance in the human body to maintain normal physiological functions and is an essential antioxidant that is widely present in

[a] C. van der Horst, B. Silwana, V. Somerset
Dep Faculdade de Farmácia, Universidade Federal de Goiás, Praça Universitára, Campus Colemar Natal e Silva, CEP: 74605-220 Goiâs,
and
Brazilartment of Chemistry, Faculty of Applied Sciences, Cape Peninsula University of Technology, Bellville, South Africa
E-mail: vsomerset@gmail.com
[b] E. Gil
Faculdade de Farmácia, Universidade Federal de Goiás, Campus Colemar Natal e Silva, Praça Universitára, CEP: 74605-220 Goiâs, Brazil
[c] E. Iwuoha
SensorLab, Department of Chemistry, University of the Western Cape,Cape Town, Bellville 7535, South Africa

Supporting information for this article is available on the WWW under https://doi.org/10.1002/elan.202060389

biological systems. Symptoms like infertility, fatigue, and scurvy are a result of abnormal concentrations of AA [26,27].

In the determination of biomolecules pharmaceutical samples, until now several techniques have been used such as UV-spectrophotometry [28], capillary electrophoresis [29], high performance liquid chromatography (HPLC) [30,31], titrimetry [32], thermogravimetric analysis (TGA) [33], and HPLC-tandem mass spectrometry [34]. These methods have several disadvantages such as poor selectivity, lower selectivity, high cost, and time-consuming. Bismuth silver bimetallic nanoparticles were chemically synthesized by Van der Horst et al. [35] for the analysis of PGMs [36–39], H_2O_2 [40], and individual detection of AA [41]. In this study, we have employed Bi–AgNPs onto normal GCE for the simultaneous electrochemical analysis of three different biomolecules in pharmaceutical samples. According to the literature, this is the first time that the sensor of GCE/Bi–AgNPs has been employed for the simultaneous electrochemical analysis of CAF, PAR, and AA in pharmaceutical samples.

2 Materials and Methods

2.1 Reagents

All analytical reagents were of the highest grade and purchase from Merck and Sigma-Aldrich and were used without further purification. The procedure employed for the synthesis of the bimetallic nanoparticles of bismuth-silver (Bi–AgNPs) was the same procedure reported elsewhere in the literature [35,36]. A 0.1 M phosphate buffer solution (PBS) at pH 5 was prepared from KH_2PO_4 and Na_2HPO_4. Stock solutions of PAR, AA, and CAF were prepared every week by using a 0.1 M PBS (pH = 5). In this study, all experimental solutions were prepared by using ultra-pure water. All electrochemical experiments were performed at ambient temperature and in an oxygen environment.

2.2 Instrumentation

Differential pulse voltammetry (DPV) and cyclic voltammetry (CV) analysis were performed with a BASi electrochemical analyzer (West Lafayette, IN 47906, USA). The Bi–AgNPs were employed to modify a disk GCE, a counter electrode (Pt wire), and a reference electrode (Ag/AgCl) was used to complete the three-electrode system. A 20 mL electrochemical cell was employed for all electrochemical experiments at ambient temperature [36].

2.3 Construction of the GCE/Bi–AgNPs Sensor

Before modification with the Bi-AgNPs, the disk GCE was cleaned with alumina (0.1 to 1.0 μm), sonicated in pure ethanol for 5 min, and then rinse with deionized water. The Bi-AgNPs were first dispersed into deionized water (1 mg in 10 mL) and sonicated for 5 min in an ultrasonic bath. A 20 μL of an aliquot Bi-AgNPs were dropped onto the clean disk GCE and the water was allowed to evaporate. All the experiments in this study were carried out in an oxygen environment and at ambient temperatures [39].

2.4 Procedure for the Determination of Biomolecules

Three pharmaceutical samples were used to study the practical applicability of the sensor consist of GCE and Bi–AgNPs for PAR, AA, and CAF determination in real sample analysis. The real sample such as med lemon was prepared by dissolving the powder in 250 ml boiling water. The sample was cooled down to room temperature and then analyzed using differential pulse voltammetry mode. An electrochemical cell with a three-electrode system and under the same experimental conditions was used to obtain the quantified results. The method of standard addition was employed for the electrochemical analysis of samples without PAR naturally found in the samples were spiked with a known amount of PAR to confirm the PAR anodic peak [41].

3 Results and Discussion

3.1 CV Characterization of GCE/Bi–AgNPs Sensor

CV was employed to investigate the electrochemical behaviours for the individual and simultaneous analysis of PAR, CAF, and AA using 50 μM concentration. Figure 1 illustrates the electrochemical responses observed at (a) clean GCE and (b) GCE/Bi–AgNPs sensor surfaces with 100 mV/s scan rate in a 0.1 M PBS (pH = 5.0). As illustrated in Figure 1A, the potential of the anodic peak for AA was observed at about +0.28 V (vs. Ag/AgCl) at the clean GCE and +0.35 V (vs. Ag/AgCl) at the GCE/Bi-AgNPs sensor surfaces. The anodic peak currents at the GCE/Bi-AgNPs sensor were greater than the anodic peak currents at the clean GCE. In the case of PAR, as illustrated in Figure 1B, the anodic peak potentials at the clean GCE were observed at +0.75 V (vs. Ag/AgCl) and +0.72 V (vs. Ag/AgCl) at the GCE/Bi-AgNPs sensor, respectively. The currents of the anodic peak at the surface of the GCE/Bi-AgNPs sensor was double the value as at the clean GCE. For CAF in Figure 1C, the anodic peak potentials were +1.55 V (vs. Ag/AgCl) and +1.45 V (vs. Ag/AgCl) at the clean GCE and GCE/Bi–AgNPs sensor surfaces, while the peak currents were also greater at the GCE/Bi–AgNPs sensor as observed at the surface of the clean GCE. In the case of the simultaneous analysis of AA, PAR, and CAF in Figure 1D, three well-defined anodic peaks were recorded at the GCE/Bi–AgNPs sensor surface with a very small peak for AA was recorded at the clean GCE. The potentials of the anodic peak were seen at +0.25 V (vs. Ag/AgCl) for AA, +0.7 V (vs. Ag/AgCl) for PAR, and +1.4 V (vs. Ag/

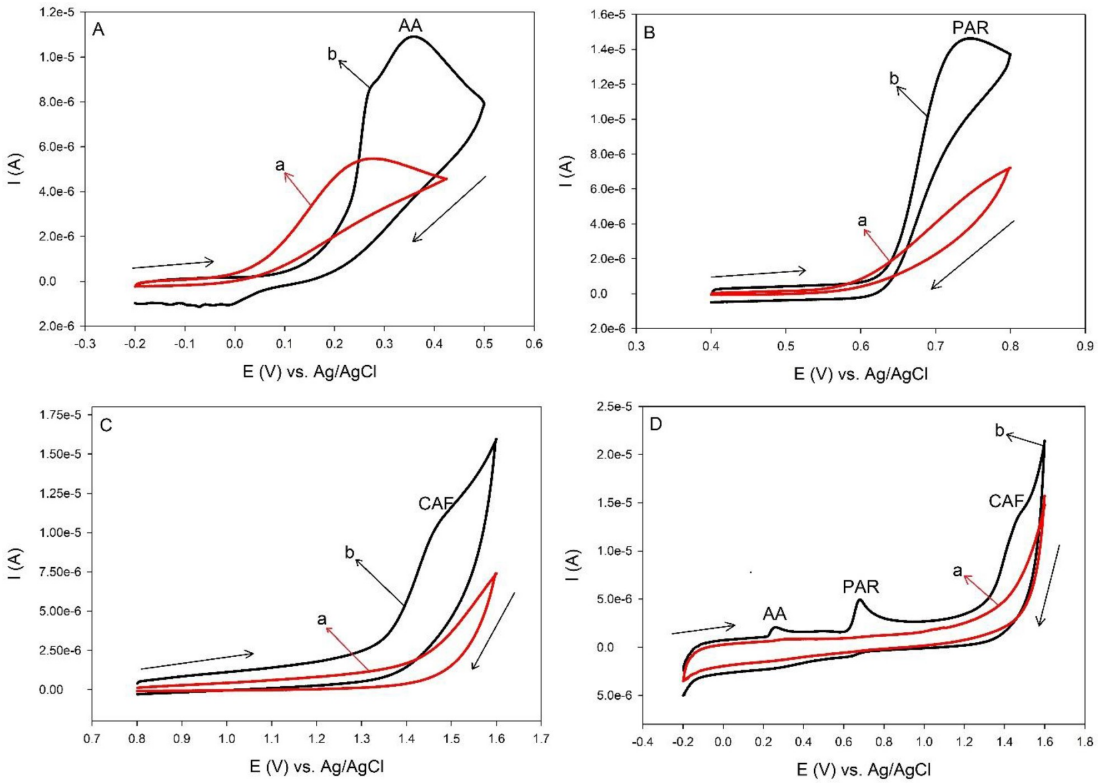

Fig. 1. CVs obtained at (a) clean GCE and (b) GCE/Bi–AgNPs in (A) AA, (B) PAR, (C) CAF and (D) simultaneous CVs for CAF, PAR, and AA in 0.1 M PBS (pH = 5.0) containing a concentration of 50 μM for AA, PAR, and CAF.

AgCl) for CAF, respectively. In the reverse scan, three cathodic peaks for AA, PAR, and CAF were recorded at the GCE/Bi–AgNPs sensor surface with one peak for AA at the clean GCE.

3.2 CV Studies of CAF, PAR, and AA at a Clean GCE and GCE/Bi–AgNPs Surfaces

Cyclic voltammetry was utilized in Figure 2 to investigate the effect of scan rate in 50 μM AA, PAR, and CAF using GCE/Bi–AgNPs sensor at scan rates of 20 to 160 mV/s. The anodic peak currents (I) of AA, PAR, and CAF increased with an increased in scan rates (V) and illustrated in Figure 2A to 2 C. The linear regression plots are illustrated in Figure 2D. The linear equation for scan rate in individual 50 μM AA can be expressed as: I_{pa}, (A) $= 2.71 \times 10^{-8} + 1.49 \times 10^{-7}$ [AA], with $R^2 = 0.985$. For PAR, the linear calibration equation can be illustrated as: I_{pa}, (A) $= 5.75 \times 10^{-9} + 6.97 \times 10^{-7}$ [PAR], with $R^2 = 0.990$. In the case of CAF, linear calibration equation is also illustrated as: I_{pa}, (A) $= 5.21 \times 10^{-9} + 4.91 \times 10^{-7}$ [CAF], with $R^2 = 0.987$. The results obtained above shown that the electrocatalytic anodic processes for AA, PAR, and CAF in this study were adsorption-controlled at the GCE/Bi–AgNPs sensor surface, suggesting the possibility of constructing a method to detect AA, PAR, and CAF using DPV.

3.3 DPV Detection of AA, PAR, and CAF Using Different Sensors

The proposed electrochemical procedure was used for the detection of CAF, PAR, and AA at the GCE/Bi–AgNPs sensor surface in a 0.1 M PBS (pH = 5). DPV was used to determine the three biomolecules in pharmaceuticals because it offers higher sensitivity and good resolution when compared to the normal cyclic voltammetry. Figure 3 illustrates the individual electrochemical analysis of (A) AA, (B) PAR, and (C) CAF using (a) clean GCE, and (b) GCE/Bi–AgNPs sensor. In Figure 3A, a small peak was observed for AA at the clean GCE surface with a well-defined peak and with an extra small peak for AA at the surface of the GCE/Bi–AgNPs sensor. The small peak is due to impurities in the 0.1 M PBS. For PAR in Figure 3B, no peak was observed for the clean GCE with a well-defined peak for PAR at the GCE/Bi–AgNPs sensor surfaces. Figure 3C shown a small flat peak for CAF at the clean GCE with a well-defined peak at the GCE/Bi–AgNPs sensor surfaces. The observed results indicate that the anodic peak currents intensities for PAR, CAF, and AA at the surface of the GCE/Bi–AgNPs sensor are greater than the intensities at the clean GCE. In the case of the simultaneous electrochemical analysis of CAF, AA, and PAR in Figure 3D, three well-defined anodic peaks were showcase at the GCE/Bi–AgNPs sensor surface. For the clean GCE, only one broad anodic

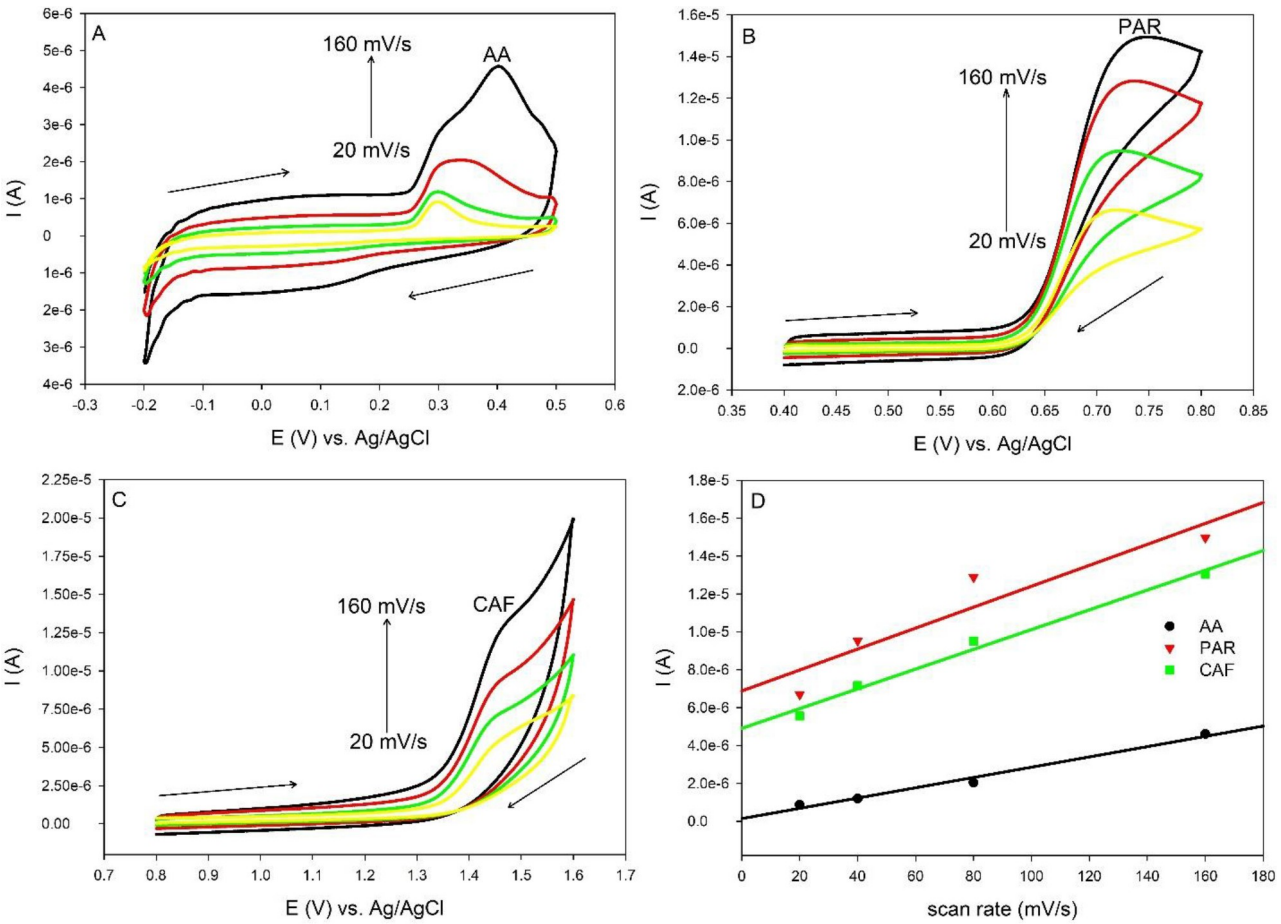

Fig. 2. CVs obtained of 50 μM AA in (A), PAR in (B), and CAF in (C) using a 0.1 M PBS (pH = 5.0) at the surface of a GCE/Bi–AgNPs sensor at various scan rates (20, 40, 80 and 160 mV/s). (D) A calibration curve of peak current versus scan rate for AA, PAR, and CAF.

peak was observed with no separations of the three biomolecules peaks. It is an indication that PAR, AA, and CAF were electrooxidized on the GCE/Bi–AgNPs sensor surface and can be used to detect PAR, AA, and CAF in model standard solutions.

3.4 Individual Determination of CAF, PAR, and AA

The quantitative determination of CAF, PAR, and AA under optimum conditions at a GCE/Bi–AgNPs sensor was done by DPV. Figure 4 illustrates the individual analysis of (A) AA, (B) PAR, and (C) CAF in a 0.1 M PBS (pH = 5.0). DPV was employed to detect AA, PAR, and CAF because it offers well-defined peaks, higher sensitivity, and good peak separation compared to CV. As illustrated, the peak current intensities of the anodic peaks for AA, PAR, and CAF increased as the concentrations increased. This is an indication that AA, PAR, and CAF were electrooxidized on the surface of a GCE/Bi–AgNPs sensor. The GCE/Bi–AgNPs sensor showcase for the individual analysis excellent electrocatalytic response for CAF, PAR, and AA at peak potentials of +1.32 (vs. Ag/AgCl), +0.54 (vs. Ag/AgCl), and +0.21 V (vs. Ag/AgCl), respectively. Figure 4D illustrates the linear regression plots for AA, PAR, and CAF, and the analytical curves also showed three good linear relationships. The anodic peak currents for AA revealed a response of linearity to the increasing concentration in a range of 10 to 50 μM. The linear equation for individual AA detection can be expressed as $I_{pa,\ AA}(\mu A) = 1.55 \times 10^{-7}\ C_{AA}\ (\mu M) + 2.02 \times 10^{-6}$ ($R^2 = 0.950$). For the currents of the oxidation peaks of PAR, a response of linearity to the increasing concentration in a range of 10 to 100 μM with a linear equation expressed as $I_{pa,\ PAR}(\mu A) = 2.06 \times 10^{-8}\ C_{PAR}\ (\mu M) + 3.21 \times 10^{-7}$ ($R^2 = 0.999$). In the case of CAF, a response of linearity in a range of 10 to 100 μM was obtained with a calibration curve equation expressed as $I_{pa,\ CAF}(\mu A) = 1.99 \times 10^{-7}\ C_{CAF}\ (\mu M) + 1.20 \times 10^{-5}$ ($R^2 = 0.984$). The detection limits for CAF, PAR, and AA were individually determined using the statistical method of LOD = 3 × SD/m, where SD is the standard deviation of blank (n = 10) and m is the slope linear plot [41]. The detection limits for CAF, PAR, and AA were 0.098, 0.068, and 0.014 μM, respectively. This GCE/Bi-AgNPs sensor could, therefore, be used for the simultaneous

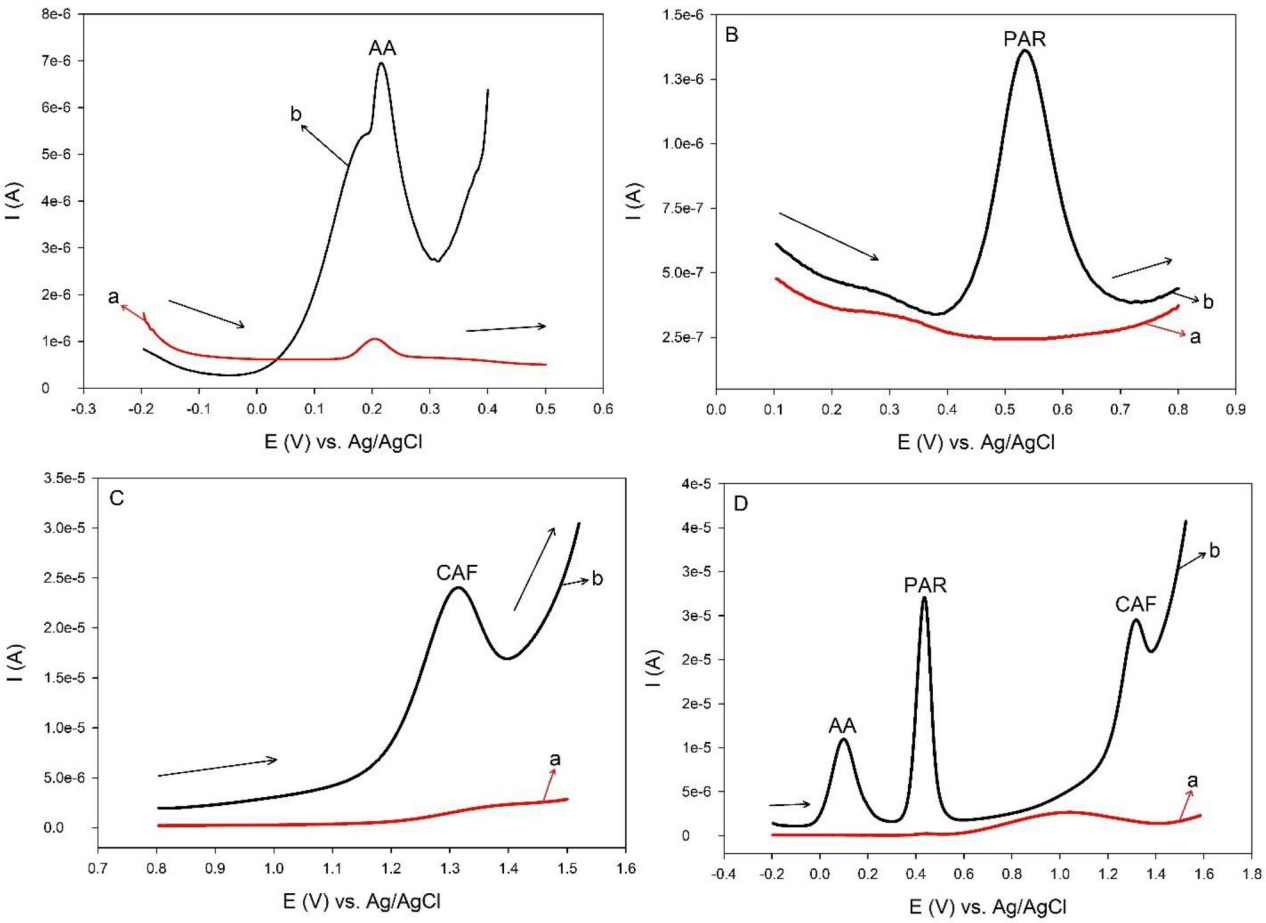

Fig. 3. DPVs obtained at (a) clean GCE and (b) the GCE/Bi–AgNPs; (A) for AA, (B) for PAR, and (C) for CAF in a 0.1 M PBS (pH = 5.0) containing a concentration of 50 μM of AA, PAR, and CAF. (D) Simultaneous DPVs for 80 μM AA, 30 μM PAR, and 80 μM CAF at (a) clean GCE and (b) the GCE/Bi–AgNPs sensor.

electrochemical analysis of CAF, PAR, and AA in model solutions using the above experimental parameters.

3.5 Detection of CAF, PAR, and AA Mixtures Using the GCE/Bi–AgNPs Sensor

In this study, well-defined peaks of the individual detection of CAF, PAR, and AA were observed under optimized experimental conditions. Another investigation was done by testing the versatility of the GCE/Bi–AgNPs working electrode for the selective detection of a solution containing CAF, PAR, and AA. Differential pulse voltammetry was employed in the analysis of a solution by keeping the concentrations of two species constant and changing the concentration of one species. As illustrated in Figure 5A, the anodic peak currents of AA increase linearly with increasing concentration from 10 to 80 μM while keeping PAR and CAF concentrations constant at 4 μM and 10 μM, respectively. The equation of the calibration curve was illustrated as I_p (μA) = 0.0154 C_{AA} (μM) + 0.0193 (R^2 = 0.989). This observation illustrates that the GCE/Bi-AgNPs electrode shown a good response to AA electrocatalytic in the presence of CAF and PAR. Figure 5B illustrates the DPVs of PAR with increasing concentrations from 2 to 30 μM with constant concentrations of 10 μM for AA and 20 μM for CAF. The calibration equation was illustrated as I_p (μA) = 0.1209 C_{PAR} (μM) + 0.4096 (R^2 = 0.995). Furthermore, the DPVs of CAF are illustrated in Figure 5C that the currents of the anodic peak linearly increase with an increase in concentrations. Caffeine concentrations were increased from 10 to 80 μM while keeping the concentrations of PAR and AA constant at 4 and 10 μM, respectively, with a linear response illustrated as I_p (μA) = 0.0245 C_{CAF} (μM) + 1.280 (R^2 = 0.997). Considering the investigations conducted above, the GCE/Bi-AgNPs sensor illustrates excellent electrocatalytic response for the detection of PAR, CAF, and AA in a pH 5.0 solution which allows the use of this sensor for the simultaneous detection of these biomolecules below. The linear regression plots of the three biomolecules are illustrated in Figure 5D. These results are illustrated in Figure 5 were compared with the results obtained in the work done by Fernandes et al. [19] and have similarities.

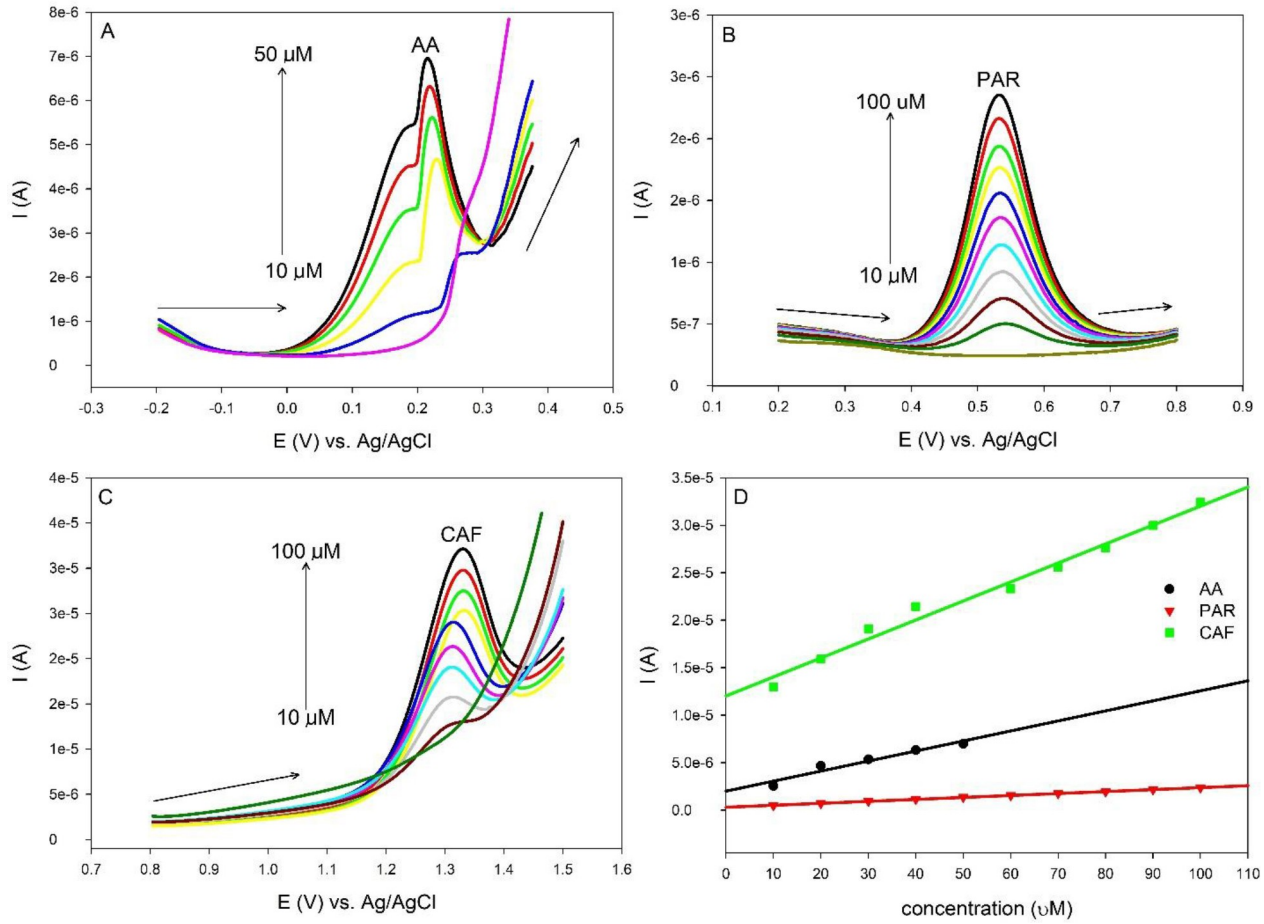

Fig. 4. Individual DPVs of GCE/Bi–AgNPs for AA (A), PAR (B), and CAF (C) with concentrations of AA ranging from 10 to 50 µM, PAR ranging from 10 to 100 µM, and CAF ranging from 10 to 100 µM, respectively, in a 0.1 M PBS (pH 5.0). In D, Calibration curves of the peak currents versus concentration of AA, PAR, and CAF.

3.6 Simultaneous Electrochemical Analysis of CAF, PAR, and AA

The DPV curves of simultaneous electrochemical analysis of CAF, PAR, and AA in a 0.1 M PBS (pH = 5.0) are illustrated in Figure 6A. The simultaneous detection of CAF, PAR, and AA was examined by varying their concentrations simultaneously. As illustrated in Figure 6A, three separated and well-defined anodic peaks for PAR, AA, and CAF are approximately at +0.42 (vs. Ag/AgCl), +0.15 V (vs. Ag/AgCl), and +1.30 V (vs. Ag/AgCl), respectively, while the anodic peak currents were also increased consistently. We observed that the currents for the oxidation peaks of AA, PAR, and CAF increased linearly as the concentrations increased. The quantity of AA ranges from 10 to 70 µM and PAR ranging from 2 to 20 µM and CAF ranging from 2 to 40 µM. These results showed that the GCE/Bi-AgNPs working electrode can be applied for the simultaneous electrochemical analysis of PAR, CAF, and AA with no interference between the molecules.

Figure 6B is an illustration of the calibration plots of the currents for the anodic peak (I_p) for PAR, AA, and CAF versus the concentrations of PAR, AA, and CAF. The currents of the anodic peaks were linearly related to the concentrations of AA, PAR, and CAF. This observation is illustrated below by the linear equations as I_p (A) $= 1.411 \times 10^{-7}$ C_{AA} (µM) $+ 1.884 \times 10^{-6}$ with $R^2 = 0.9813$ for AA, I_p (A) $= 1.336 \times 10^{-6}$ C_{PAR} (µM) $+ 1.356 \times 10^{-6}$ with $R^2 = 0.9655$ for PAR, and I_p (A) $= 3.282 \times 10^{-7}$ C_{CAF} (µM) $+ 1.200 \times 10^{-7}$ with $R^2 = 0.9937$ for CAF. We observed that the values of the slope of AA, PAR, and CAF recorded in the simultaneous detection are not similar compared to individual detection of these biomolecules. The results obtained during the simultaneous electrochemical analysis of CAF, PAR, and AA illustrate that they did not interfere with each other. Table 1 is an illustration of the performance for the GCE/Bi-AgNPs sensor for AA, PAR, and CAF detections compared with other modified electrodes. This modified GCE/Bi-AgNPs sensor has a comparable detection limit for AA, PAR, and CAF detection compared with other modified electrodes.

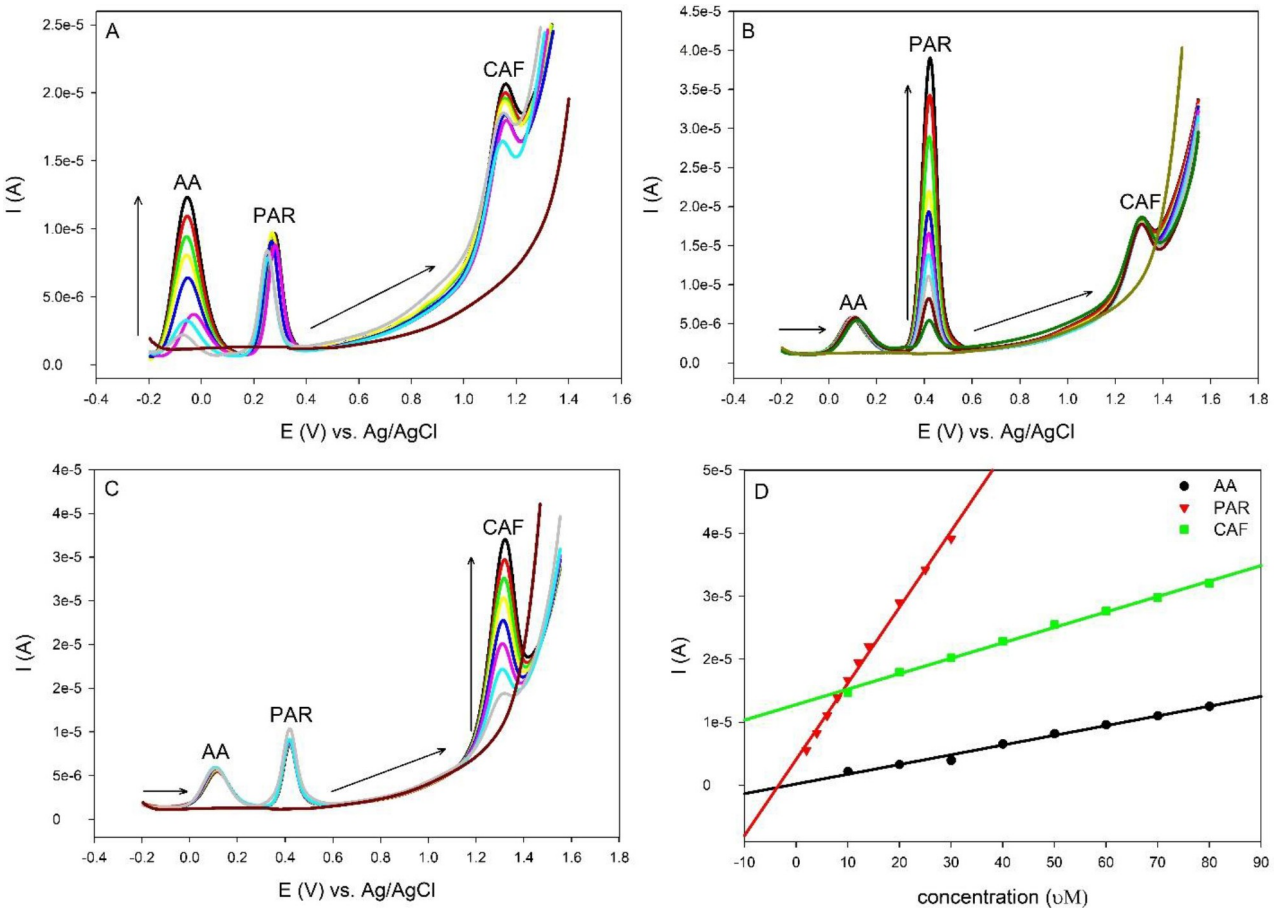

Fig. 5. (A) DPVs at the GCE/Bi–AgNPs in a 0.1 M PBS (pH = 5.0) consist of AA at concentrations range from 10 to 70 μM, 4 μM for PAR and 20 μM for CAF, (B) DPVs at the GCE/Bi–AgNPs for PAR at concentrations ranging from 2 to 30 μM, consist of 10 μM AA and 20 μM CAF, in a 0.1 M PBS (pH = 5.0). (C) DPVs at the surface of a GCE/Bi–AgNPs for CAF at concentrations ranging from 10 to 80 μM, containing 4 μM PAR and 20 μM CAF, in a 0.1 M PBS (pH = 5.0). (D) A calibration curve of current intensity versus the concentration of CAF, PAR, and AA.

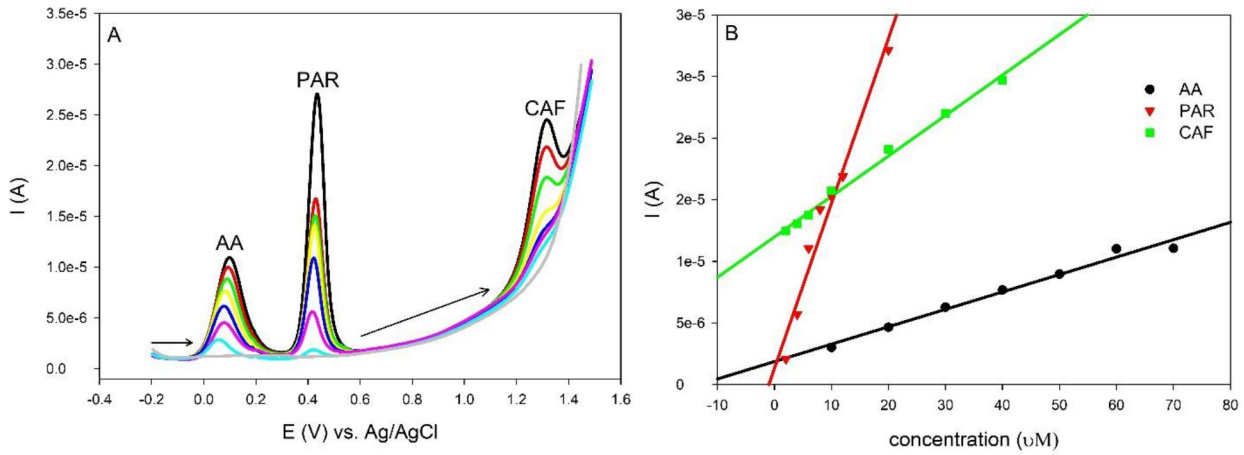

Fig. 6. A. An illustration of the simultaneous DPV for CAF, AA, and PAR at the GCE/Bi-AgNPs. DPVs for the increasing of individual concentrations of AA, PAR, and CAF. PAR concentrations ranged from 2 to 30 μM and concentrations of AA and CAF ranged from 10 to 80 μM, in a 0.1 M PBS (pH = 5.0). B, Calibration plots of the GCE/Bi–AgNPs sensor for AA, PAR, and CAF, respectively.

Table 1. An illustration of the application of different electroactive materials employed to construct electrochemical sensors for the electrochemical analysis of CAF, PAR, and AA.

Material	Method	Analyte	Linear ranges (μM)	Detection limits (μM)	References
$MnFe_2O_4$@CNT-N	SWV	AA	2–100	1.8	[19]
		PAR	1–1000	0.83	
		CAF	1–1100	0.83	
Bi/Nafion/BDDE	DPV	PAR	0.2–500	0.036	[18]
		CAF	0.01–20	0.0028	
PNBM	DPV	PAR	0.2–16.2	0.08	[42]
		CAF	0.8–19.7	0.1	
CuNPs-GO-CB-PEDOT:PSS	SWV	PAR	0.9–7.0	0.23	[43]
		CAF	11–64	3.4	
PEDOT/h-CN/GCE	DPV	AA	4–20, 20–1800	1.51	[44]
		PAR	1–10, 10–50	0.49	
GORGCP	DPV	CAF	8–800	0.153	[45]
MWCNT/GCE		PAR	0.0002–15	0.09	[46]
SiO_2/MWCNT	DPV	PAR	0.5–6.0	0.098	[47]
		UA	0.5–10.0	0.068	
GCE/Bi-AgNPs	DPV	AA	10–70	0.697	This work
		PAR	2–20	0.155	
		CAF	2–40	2.36	

3.7 Interference Studies

In the human body, uric acid (UA) and neurotransmitters are important interferences. In this investigation, the sensitivity of Bi–AgNPs sensor in the presence of some potential interfering ions (uric acid, fructose, glucose), the DPV current responses of successive additions of AA, PAR, and CAF were recorded in PBS (pH 5), containing 20 μM UA, 10 μM AA, 5 μM PAR, and 10 μM CAF respectively (Figure 7). These interfering compounds do not interfere with AA, PAR, and CAF when GCE/Bi-AgNPs sensor was used.

3.8 Repeatability and Stability Test of GCE/Bi–AgNPs

The three parameters such as reproducibility, stability, and repeatability were investigated using mixtures of 50 μM concentrations of PAR, AA, and CAF solutions. The RSDs of six replicate measurements for PAR, AA, and CAF mixture solutions were 2.53 %, 3.61 %, and 4.91 %, respectively, which indicates that the GCE/Bi-AgNPs sensor has good repeatability. In the case of reproducibility, four different GCE/Bi-AgNPs sensors were prepared for the electrochemical testing of 50 μM concentrations of PAR, AA, and CAF in a solution of phosphate buffer (pH = 5.0). The RSDs were to be 2.53 % for AA, 3.11 % for PAR, and 2.89 % for CAF, respectively, which illustrates excellent reproducibility. The test for stability of the constructed procedure was also performed, the current of the anodic peak for CAF, PAR, and AA recorded shown a decrease of 6 % after the GCE/Bi-AgNPs were put in storage at 5 °C for fourteen days. This evidence illustrates the GCE/Bi-AgNPs sensor has good stability.

3.9 Practical application of GCE/Bi–AgNPs sensor

The practical application of the proposed procedure was tested by the electrochemical analysis of the contents of CAF, AA, and PAR in pharmaceutical formulations by the addition and recovery experiments. The GCE/Bi–AgNPs sensor was employed to detect PAR, CAF, and AA in real med lemon formulae. The amount of AA, PAR, and CAF in the real med lemon formulae were found to be 43.9 mg, and 48.7 mg indicating an agreement with the concentration of AA, and CAF given by the composition values. A known amount of 10 mg PAR was added to the med lemon sample and 9.8 mg PAR was recover by the sensor. Clearly, the proposed method illustrates the applicability and reliability of the GCE/Bi–AgNPs sensor with mean recoveries in the range of 97.6, 97.4, and 98.0 % for AA, CAF, and PAR, respectively. These results (Table 2) obtained by the electrochemical sensor showed that the Bi–AgNPs have excellent analytical performance, and might be an alternative material in the development and construction of electro-

Table 2. Illustration of the results for the electrochemical analysis of CAF, PAR, and AA in med lemon.

Analyte	Labeled (mg)	Spiked quantity (mg)	Found (mg)	% Recovery	% RSD
AA	45	0	43.9	97.6	3.67
CAF	50	0	48.7	97.4	2.41
PAR	0	10	9.8	98.0	5.07

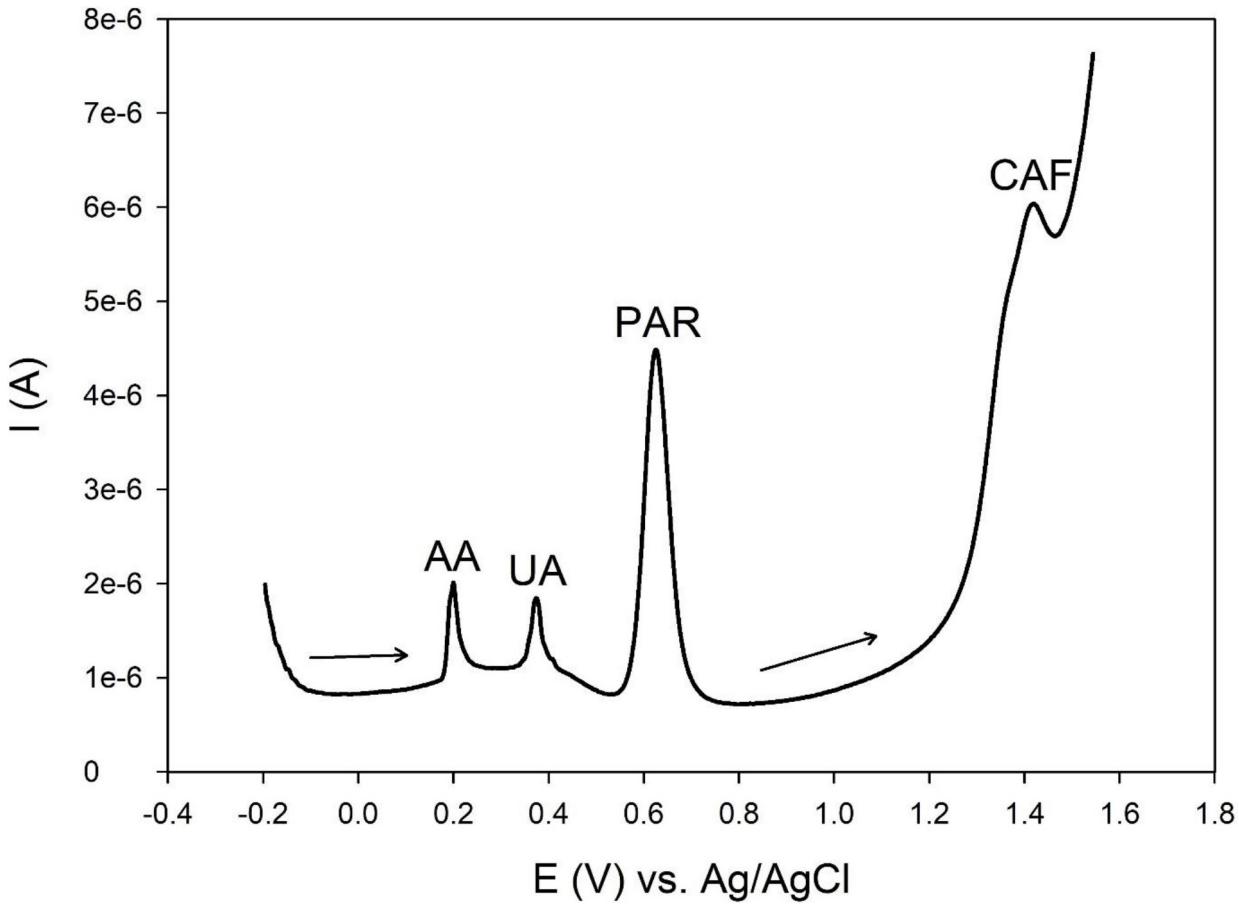

Fig. 7. An illustration for the interference study of UA, fructose and glucose with CAF, AA, and PAR at the GCE/Bi-AgNPs.

chemical sensors for the electrochemical analysis of PAR, CAF, and AA in commercial pharmaceutical formulae.

4 Conclusion

The GCE/Bi-AgNPs electrochemical sensor feasibility in the determination of biomolecules in pharmaceutical formulae by DPV was confirmed. The Bi–AgNPs was drop coated as a thin film onto a GCE surface, this GCE/Bi-AgNPs, illustrated excellent electrocatalytic response for both the simultaneous and individual detection of CAF, PAR, and AA with low limits of detection. The proposed procedure using bimetallic nanosensor illustrates very good peak separation of AA, PAR, and CAF with peak potentials of +100 mV, +430 mV, and +1300 mV respectively. This sensor also illustrated excellent electrocatalytic response for these biomolecules in pharmaceutical formulae with no interference between them and other species. These characteristics with robustness illustrated by the sensor, revealed that they can be applicable in real sample analysis of CAF, PAR, and AA.

Acknowledgements

This investigation was financially supported by the Cape Peninsula University of Technology (CPUT). The authors also acknowledge the Council for Scientific and Industrial Research (CSIR), Stellenbosch, South Africa.

Data Availability Statement

The data that support the findings of this study are available from the corresponding author upon reasonable request.

References

[1] R. H. Baughman, A. A. Zakhidov, W. A. de Heer, *Sci. J.* **2002**, *297*, 787–792.
[2] D. Eder, *Chem. Rev.* **2010**, *110*, 1348–1385.
[3] J. S. Wu, W. Pisula, K. Mullen, *Chem. Rev.* **2007**, *107*, 718–747.
[4] M. D. Stoller, S. J. Park, Y. W. Zhu, J. H. An, R. S. Ruoff, *Nano Lett.* **2008**, *8*, 3498–3502.
[5] Y. Wang, Z. Q. Shi, Y. Huang, Y. F. Ma, C. Y. Wang, M. M. Chen, Y. S. Chen, *J. Phys. Chem. C* **2009**, *113*, 13103–13107.
[6] M. J. Allen, V. C. Tung, R. B. Kaner, *Chem. Rev.* **2010**, *110*, 132–145.

[7] D. Chen, L. H. Tang, J. H. Li, *Chem. Soc. Rev.* **2010**, *39*, 3157–3180.
[8] H. Jang, Y. J. Park, X. Chen, T. Das, M.-S. Kim, J.-H. Ahn, *Adv. Mater.* **2016**, *28*, 4184–4202.
[9] J. Lu, Z. Chen, Z. Ma, F. Pan, L. A. Curtiss, K. Amine, *Nat. Nanotechnol.* **2016**, *11*, 1031–1038.
[10] A. Pandikumar, G. T. Soon How, T. P. See, F. S. Omar, S. Jayabal, K. Z. Kamali, N. Yusoff, A. Jamil, R. Ramaraj, S. A. John, H. N. Lim, N. M. Huang, *RSC Adv.* **2014**, *4*, 63296–63323.
[11] K. Bindu, K. Sridharan, K. Ajith, H. Lim, H. Nagaraja, *Electrochim. Acta* **2016**, *217*, 139–149.
[12] H. Wang, F. Ren, C. Wang, B. Yang, D. Bin, K. Zhang, Y. Du, *RSC Adv.* **2014**, *4*, 26895–26901.
[13] H. Sun, H. Li, I. Harvey, P. J. Sadler, *J. Biochem.* **1999**, *274*, 29094–29101.
[14] H. Guo, Y. Li, P. Xiao, N. He, *Anal. Chim. Acta* **2005**, *534*, 143–47.
[15] S. B. Hočevar, B. Ogorevc, J. Wang, B. Pihlar, *Electroanalysis* **2002**, *14*, 1707–1712.
[16] G. Kefala, A. Economou, M. Sofoniou, *Talanta* **2006**, *68*, 1013–1019.
[17] J. Wang, D. Lu, S. Thongngamdee, Y. Lin, O. Sadik, *Talanta* **2006**, *69*(4), 914–917.
[18] I. Sadok, K. Tyszczuk-Rotko, A. Nosal-Wiercinska, *Sens. Actuators B* **2016**, *235*, 263–272.
[19] D. M. Fernandes, N. Silva, C. Pereira, C. Moura, J. M. C. S. Magalhães, B. B. Baeza, I. Rodríguez-Ramos, A. Guerrero-Ruiz, C. Delerue-Matos, C. Freire, *Sens. Actuators B* **2015**, *218*, 128–136.
[20] C. Gaidau, A. Petica, C. Ciobanu, T. Martinescu, *Biotechnol. Lett.* **2009**, *14*(5), 4665–4672.
[21] V. K. Shukla, R. S. Yadav, P. Yadav, A. C. Pandey, *J. Hazard. Mater.* **2012**, *213–214*, 161–166.
[22] L. Y. Shiroma, M. Santhiago, A. L. Gobbi, L. T. Kubota, *Anal. Chim. Acta* **2012**, *725*, 44–50.
[23] D. Sun, H. Zhang, *Microchim. Acta.* **2007**, *158*, 131–136.
[24] A. A. Aly, *Food Sci. Quality Management* **2013**, *22*, 28–34.
[25] S. Guo, Q. Zhu, B. Yang, J. Wang, B. Ye, *Food Chem.* **2011**, *129*, 1311–1314.
[26] B. Habibi, M. Abazari, M. P. Azar, *Chinese J. Catalysis* **2012**, *33*, 1783–1790.
[27] Z. H. Sheng, X. Q. Zheng, J. Y. Xu, W. J. Bao, F. B. Wang, X. H. Xia, *Biosens. Bioelectron.* **2012**, *34*, 125–131.
[28] C. Wang, J. Du, H. Wang, C. E. Zou, F. Jiang, P. Yang, Y. Du, *Sens. Actuators B* **2014**, *204*, 302–309.
[29] N. G. Tsierkezos, S. H. Othman, U. Ritter, L. Hafermann, A. Knauer, J. M. Köhler, C. Downing, E. K. Mccarthy, *Sens. Actuators B* **2016**, *231*, 218–229.
[30] G. Abirami, T. Vetrichelvan, *Int. J. Pharm. Pharm. Sci.* **2013**, *5*, 488–492.
[31] Q. Chu, L. Jiang, X. Tian, J. Ye, *Anal. Chim. Acta* **2008**, *606*, 246–251.
[32] M.-H. Langlois, A. Vekris, C. Bousses, E. Mordelet, N. Buhannic, C. Séguard, *J. Chrom. B* **2015**, *988*, 20–24.
[33] M. Khanmohammadi, M. Soleimani, F. Morovvat, A. B. Garmarudi, M. Khalafbeigi, K. Ghasemi, *Thermochim. Acta* **2012**, *530*, 128–132.
[34] H. Modick, A. Schütze, C. Pälmke, T. Weiss, T. Brüning, H. M. Koch, *J. Chromatogr. B* **2013**, *925*, 33–39.
[35] C. Van der Horst, B. Silwana, E. Iwuoha, V. Somerset, *Anal. Lett.* **2015** a, *48*, 1–22.
[36] C. Van der Horst, B. Silwana, E. Iwuoha, V. Somerset, *J. Electroanal. Chem.* **2015** b, *752*, 1–11.
[37] C. Van der Horst, B. Silwana, E. Iwuoha, V. Somerset, *J. Nano Res.* **2016** a, *44*, 126–133.
[38] C. Van der Horst, B. Silwana, E. Iwuoha, V. Somerset, *Voltammetric Analysis of Platinum Group Metals Using a Bismuth-Silver Bimetallic Nanoparticles Sensor*, Rahman, M. M., Asiri, A. M. (ed.), Recent Progress in Organometallic Chemistry, INTECH, Croatia, **2017**.
[39] C. Van der Horst, B. Silwana, E. Iwuoha, V. Somerset, *Environment* **2018**, *5*, 120.
[40] C. Van der Horst, B. Silwana, E. Iwuoha, V. Somerset, *Proc. Technol.* **2017**, *27*, 179–182.
[41] C. Van der Horst, B. Silwana, E. Iwuoha, E. Gil, V. Somerset, *Food Anal. Methods* **2016** b, *9*, 2560–2566.
[42] S. Chitravathi, N. Munichandraiah, *J. Electroanal. Chem.* **2016**, *764*, 93–103.
[43] A. Wong, A. Martin Santos, T. Almeida Silva, O. Fatibello-Filho, *Talanta* **2018**, *183*, 329–338.
[44] C. Li, J. Xu, Y. Wu, Y. Zhang, C. Zhang, W. Lei, Q. Hao, *J. Electroanal. Chem.* **2018**, *824*, 52–59.
[45] M. Shehata, S. M. Azab, A. M. Fekry, *Synth. Met.* **2019**, *256*, 116–122.
[46] A. Kutluay, M. Aslanoglu, *Sens. Actuators B* **2016**, *185*, 398–404.
[47] T. C. Canevari, P. A. Raymundo-Pereira, R. Landers, E. V. Benvenutti, S. A. S. Machado, *Talanta* **2013**, *116*, 726–735.

Received: September 28, 2020
Accepted: October 7, 2020
Published online on November 4, 2020

